



Numerical Study of the Instability and Flow Transition in a Vortex-Ring/Wall Interaction

H. Ren[†], G. X. Zhang and H. S. Guan

China Electronics Technology Group Corporation No.38 Research Institute, Hefei 230088, P.R. China

[†] Corresponding Author Email: renheng_cetc38@163.com

(Received April 19, 2015; accepted September 20, 2015)

ABSTRACT

Instability and flow transition of a vortex ring impinging on a wall were investigated by means of large-eddy simulation for two vortex core thicknesses corresponding to thin and thick vortex rings. Various fundamental mechanisms dictating the flow behaviours, such as evolution of vortical structures, instability and breakdown of vortex rings, development of modal energies, and transition from laminar to turbulent state, have been studied systematically. Analysis of the enstrophy of wrapping vortices and turbulent kinetic energy (TKE) in flow field indicates that the formation and evolution of wrapping vortices are closely associated with the flow transition to turbulent state. It is found that the temporal development of wrapping vortices and the growth rate of axial flow generated around the circumference of the core region for the thin ring are faster than those for the thick ring. The azimuthal instabilities of primary and secondary vortex rings are analysed and the development of modal energies reveals the flow transition to turbulent state. The law of energy decay follows a characteristic $k^{-5/3}$ law, indicating that the vortical flow has become turbulent. The results obtained in this study provide physical insight into the understanding of the instability mechanisms relevant to the vortical flow evolution.

Keywords: Large eddy simulation; Vortical structure; Instability; Transition; Turbulent flow.

1. INTRODUCTION

Vortex rings widely exist in nature and engineering and can be considered as one typical vortex motion (Shariff and Leonard 1992). The interaction of a vortex ring with a flat wall has been studied numerically and experimentally (e.g. Boldes and Ferreri 1973; Walker *et al.* 1987; Orlandi 1990; Lim *et al.* 1991; Chu *et al.* 1993; Fabris *et al.* 1996; Cheng *et al.* 2010; Couch and Krueger 2011). However, these studies are mainly limited to relatively low-Reynolds-number flow regime and the highest Reynolds number in these studies is about 2840 (Walker *et al.* 1987). The experimental study (Walker *et al.* 1987) has revealed that the primary vortex ring no longer remains stable as it approaches the wall at high Reynolds number. When the Reynolds number is high enough, the interaction can lead to the breakdown of vortex rings and transition to turbulent state (Orlandi and Verzicco 1993; Archer *et al.* 2010). Thus, the instability of vortex rings

and transition to turbulence need to be investigated for a vortex ring impinging on a wall in the high-Reynolds-number regime.

The evolution of a free vortex ring is a prototypical vortical flow relevant to some fundamental behaviours, such as growth, instability, breakdown and transition of vortex ring. Extensive investigations have been carried out theoretically (Crow 1970; Widnall *et al.* 1974; Widnall and Tsai 1977), experimentally (Widnall and Sullivan 1973; Dazin *et al.* 2006; Gan *et al.* 2011), and numerically (Shariff *et al.* 1994; Bergdorf *et al.* 2007; Archer *et al.* 2008). Krutzsch (1939) first studied the instability of vortex ring and found that the vortex ring becomes unstable with some stationary waves distributed around its azimuthal direction. Crow (1970) investigated the aircraft trailing vortices and presented the development process of the vortex instability. Then Widnall and Sullivan (1973) verified experimentally that the stationary azimuthal waves grow in the surface at 45°

relative to the propagation direction of vortex ring, and the wave number depends on the slenderness ratio of core radius to ring radius. Widnall and Tsai (1977) gave the theoretical explanation of the instability and indicated that a straining field in the neighbourhood of the vortex core leads to the amplification of small perturbation. Shariff *et al.* (1994) established a viscous correction to the growth rate proposed by Widnall and Tsai (1977) based on their direct numerical simulation (DNS) results. Dazin *et al.* (2006) experimentally investigated the linear and nonlinear stages of vortex ring decay and noticed that the straining field causes the instability. Bergdorf *et al.* (2007) numerically studied the evolution of vortex rings at $Re_\Gamma = 7500$ based on the circulation of the vortex ring and demonstrated the formation of a series of hair-pin vortices during the early turbulent stage. Archer *et al.* (2008) further investigated the effects of Reynolds number and core thicknesses on the vortex ring evolution from laminar to the early turbulent regime and indicated that the onset of the turbulent state is associated with the formation of a series of hairpin vortices.

Compared with the studies of the instability of free vortex rings, the investigation relevant to the instability of a vortex ring impinging on a wall is still scarce. Walker *et al.* (1987) experimentally investigated the vortical structures at $564 \leq Re \leq 2840$. They observed that the wavelike instability of vortical structures is generated and the ejection of secondary vortex ring is formed at high Reynolds number. Orlandi and Verzicco (1993) numerically analysed the azimuthal instabilities at $Re = 1250$ by imposing an initial azimuthal perturbation on the primary vortex ring and identify a response perturbation in the secondary ring. Archer *et al.* (2010) then studied a laminar vortex ring impacting a free surface using direct numerical simulation (DNS) and found that the instability transfers from short-wavelength instability to long-wavelength instability. The transfer happens through the rotation of wavy inner core structure and the shedding of outer core vorticity. Recently, Masuda *et al.* (2012) and Yoshida *et al.* (2012) experimentally studied the interaction of a vortex ring with a granular layer at $1500 \leq Re \leq 4100$. They found that the wavy secondary vortex ring develops into hair-pin vortices and the hair-pin vortices then wrap around the primary vortex ring in the late stage of the interaction.

In this paper, large eddy simulation is utilized to investigate the instability and flow transi-

tion of a vortex ring impinging on a wall at high Reynolds number $Re = 4 \times 10^4$. The purpose is to achieve an improved understanding of some of the fundamental phenomena involved in this flow, including evolution of vortical structures, instability of primary and secondary vortex rings, breakdown of vortex rings, and transition of the flow from laminar to turbulent regime.

2. MATHEMATICAL FORMULATION AND NUMERICAL METHODS

To investigate a vortex ring impinging on a flat wall, the three-dimensional Favre-filtered compressible Navier-Stokes equations in generalized coordinates are used. The equation of state for an ideal gas is used and the molecular viscosity is assumed to obey the Sutherland law. We use the far-field variables and the initial radius of vortex ring to non-dimensionalize the equations, which can be expressed as

$$\frac{\partial \bar{\rho}}{\partial t} + \frac{\partial(\bar{\rho}\bar{u}_i)}{\partial x_i} = 0, \quad (1)$$

$$\frac{\partial(\bar{\rho}\bar{u}_i)}{\partial t} + \frac{\partial(\bar{\rho}\bar{u}_i\bar{u}_j)}{\partial x_j} = -\frac{\partial \bar{p}}{\partial x_i} + \frac{\partial(\bar{\tau}_{ij} - \tau_{ij}^{SGS} + D_{ij}^{SGS})}{\partial x_j}, \quad (2)$$

$$\begin{aligned} \frac{\partial \bar{\rho}\bar{E}}{\partial t} + \frac{\partial[(\bar{\rho}\bar{E} + \bar{p})\bar{u}_i]}{\partial x_i} = & \frac{\partial}{\partial x_i}(-\bar{q}_i + \bar{u}_j\bar{\tau}_{ij} + \mathcal{J}_i^{SGS} \\ & + \sigma_i^{SGS} - Q_i^{SGS} - H_i^{SGS}), \end{aligned} \quad (3)$$

where an overbar denotes the spatial filter and a tilde the Favre filter. The variables ρ , u_i , p and E represent the density, velocity component, pressure and specific total energy, respectively. The diffusive fluxes are given by

$$\bar{\tau}_{ij} = 2\bar{\mu}\bar{S}_{ij} - \frac{2}{3}\bar{\mu}\delta_{ij}\bar{S}_{kk}. \quad (4)$$

The subgrid closure terms in equations (2) and (3) are defined as

$$\tau_{ij}^{SGS} = \bar{\rho}(\widetilde{u_i u_j} - \bar{u}_i \bar{u}_j), \quad (5)$$

$$H_i^{SGS} = C_p \left(\bar{\rho} \widetilde{u_i T} - \bar{\rho} \bar{u}_i \bar{T} \right), \quad (6)$$

$$\mathcal{J}_i^{SGS} = -\frac{1}{2} \bar{\rho} (\widetilde{u_i u_k u_k} - \bar{u}_i \bar{u}_k \bar{u}_k), \quad (7)$$

$$D_{ij}^{SGS} = (\bar{\tau}_{ij} - \tau_{ij}^{SGS}), \quad (8)$$

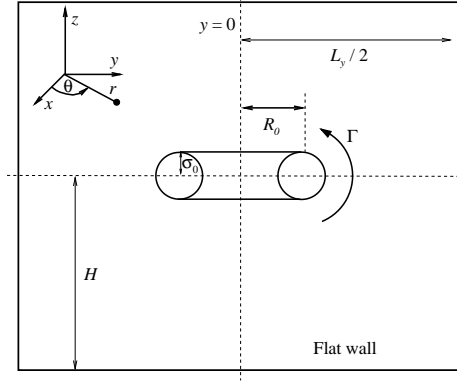


Fig. 1. Schematic diagram of a vortex ring approaching a flat wall.

$$Q_i^{SGS} = \bar{q}_i - \tilde{q}_i, \quad (9)$$

$$\sigma_i^{SGS} = (\overline{u_j \tilde{v}_{ij}} - \tilde{u}_j \tilde{v}_{ij}). \quad (10)$$

In order to model the subgrid closure terms, dynamic Smagorinsky model for compressible flows proposed by Moin *et al.* (1991) is employed. The anisotropic part of the dynamic subgrid-scale (SGS) stresses is treated by using the Smagorinsky model (Smagorinsky 1963), while the isotropic part is modelled with a formulation proposed by Yoshizawa (1986). A detailed description of the SGS models have been given in the previous paper (Moin *et al.* 1991).

The governing equations are numerically solved by a finite-volume method. As employed in our previous work (Ren *et al.* 2015), the convective terms are discretized by a second-order centered scheme and the viscous terms by a fourth-order central scheme. The time advancement is performed using an implicit approximate-factorization method with sub-iterations to ensure the second-order accuracy.

3. COMPUTATIONAL OVERVIEW AND VALIDATION

3.1 Computational Overview

As shown in Fig. 1 for the sketch of a vortex ring impacting on a wall, a vortex ring with radius R_0 is initially placed at $\mathbf{x}_c = (0, 0, H)$, where H is the distance between the vortex ring center and the wall. The initial vorticity distribution of the vortex ring is assigned by a Gaussian function and initial translational speed of

the ring can be estimated as (Saffman 1978)

$$u_s = \frac{\Gamma_0}{4\pi R_0} \left(\ln \frac{8R_0}{\sigma_0} - \frac{1}{4} \right), \quad (11)$$

where σ_0 is the initial core radius and Γ_0 is the initial circulation of vortex ring. To deal with the instability of the vortex ring, an azimuthal disturbance is introduced by imposing a radial displacement on the axis of the ring and the local radius $R(\theta)$ can be expressed as (Archer *et al.* 2008)

$$R(\theta) = R_0[1 + \zeta g(\theta)], \quad (12)$$

$$g(\theta) = \sum_{n=1}^N A_n \sin(n\theta) + B_n \cos(n\theta), \quad (13)$$

where ζ is a small parameter and is chosen as 2×10^{-4} by following the previous selection (Bergdorf *et al.* 2007; Archer *et al.* 2008), and $g(\theta)$ represents the sum of a set of N Fourier modes with $N = 32$ used here.

In the present study, we consider two typical cases for thin and thick vortex rings with the slenderness ratio $\sigma_0/R_0 = 0.2$ and 0.4 , respectively. For both the cases, the Reynolds number based on the initial translational speed and diameter of the vortex ring is $Re = 4 \times 10^4$. Based on our tests, the computational domain extends for $16R_0$ in the x - and y -directions and $12R_0$ in the vertical or z -direction, i.e. $L_x = L_y = 16R_0$ and $L_z = 12R_0$. The time step is chosen as $\Delta t = 0.005$. The grid-spacing is uniform in the x - and y -directions, and grid stretching is employed in the z -direction to increase the grid resolutions near the wall surface. The minimum size of the grid is $\Delta z = 10^{-5}R_0$. It is ensured that there are at least 40 nodes in the vorticity thickness on the wall in the attached boundary-layer region. The vortex rings are initially placed at $H = 6R_0$. Following the previous treatment (Swearingen *et al.* 1995; Archer *et al.* 2010), periodic boundary conditions are used in the x - and y -directions. The computational domain chosen in the present study is sufficiently large to ensure that the effects of the periodicity are very small. No-slip boundary condition is employed on the wall and a far-field boundary condition is applied at $z = L_z$.

3.2 Validation

To validate the present simulation, we investigate the instability of free thin and thick vortex rings and compare with the numerical results of Shariff *et al.* (1994) and Archer *et al.* (2008).

As listed in Table 1 for two vortex rings, we have obtained the most amplified mode $k = 9$ for the thin ring and $k = 6$ for the thick ring, which are the same as the previous results. Moreover, the agreement is also established in table 1 by comparison the present growth rate with the viscous correction α_S and α_A obtained by Shariff *et al.* (1994) and Archer *et al.* (2008), respectively, where the growth rate for mode k is defined as $\alpha_k = (dE_k/dt)/(2E_k)$ with E_k the perturbation energy of the mode.

Table 1 Comparison of the present growth rate α with the viscous prediction α_S of Shariff *et al.* (1994) and α_A of Archer *et al.* (2008) at $t = 52.5$

Case	σ_0/R_0	Re_Γ	k	α	α_S	α_A
A	0.200	7500	9	0.116	0.119	0.112
B	0.413	5500	6	0.080	0.090	0.072

4. RESULTS AND DISCUSSION

4.1 Vortical Structures

The evolutions of vortical structures for the thin vortex ring are shown in Fig. 2. When the vortex ring moves close to the wall, a thin vorticity layer is generated on the wall. Then, the stretching and deformation of the primary ring occur. Further, the formed vorticity layer on the wall grows rapidly due to the radially adverse pressure gradient induced by the primary ring, and results in the generation of secondary vortex ring and lifting up from the wall, as shown in Fig. 2(a). The interaction of the secondary and primary rings decelerates the expansion of the primary ring and induces the primary ring to rebound from the wall in Fig. 2(b). Then, the secondary vortex ring penetrates into the interior of the primary ring as shown in Figs. 2(c,d). Due to the growth of the azimuthal perturbation, the secondary ring evolves into a wavy-like structure. Meanwhile, a tertiary vortex ring and the induced vorticity layer separated from the wall are formed. During the above process, the strong azimuthal instability leads to the large deformation of the secondary ring. The strength and wavenumber of the azimuthal instability of primary and secondary vortex rings will be analysed in detail below. Moreover, it is observed from Figs. 2(d) and 2(e) that a series of loop-like vortices (Krishnamoorthy and Marshall 1998; Krishnamoorthy *et al.* 1999; Gossler and Marshall 2001) and hair-pin vortices (Hon and Walker 1991; Adrian 2007; Liu and Chen 2011) wrapping around the vortex rings are formed. With the evolution of vortical structures, it is seen that the strength and number of the wrapping vortices are increased con-

siderably as shown in Figs. 2(e,f). Finally, the complicated interactions of the vortex rings as well as the hair-pin and loop-like vortices in the flow field lead to the vortical structures breakdown into the small-scale vortices, and further result in the vortical flow transition to turbulent state which will be analysed below.

For the thick vortex ring, the formation of the secondary vortex ring is similar to that for the thin vortex ring case described above. After the secondary ring locates above the primary ring, it moves far away from the wall and gradually shrinks over the primary ring, as shown in Figs. 3(a,b). Correspondingly, the azimuthal instabilities of the primary and secondary rings are strengthened and the loop-like vortices wrapping around the vortex rings are enhanced during the evolution. Finally, the complicated interactions of these vortices induce the breakdown of vortices and the flow transition to turbulent state, as shown in Fig. 3(d).

Comparing the evolution of vortical structures for the thin and thick vortex rings, the secondary ring moves toward the wall for the thin ring and away the wall for the thick ring, consistent with the experimental findings for high Reynolds number (Walker *et al.* 1987). The different properties are associated with the translational velocity of the secondary ring induced by the primary ring. Moreover, the temporal development of a series of loop-like and hair-pin vortices wrapping around the rings for the thin vortex ring is faster than that for the thick vortex ring. This behaviour indicates that the instability for the thin ring evolves faster than one for the thick ring, consistent with the prediction of free vortex rings (Archer *et al.* 2008).

4.2 Instability of Vortex Rings

The perturbation growth relevant to the azimuthal instability is analysed in the early stage of a vortex ring impinging on a wall. Based on the previous analysis (Shariff *et al.* 1994, Archer *et al.* 2010), we use the root mean square value of the azimuthal velocity $u_{\theta rms}$ of vortex ring to indicate the alignment of the wavy perturbation. Fig. 4. shows the contours of $u_{\theta rms}$ for the thin ring. At $t = 15$ in Fig. 4(a), the ring is somewhat far away from the wall. It can be observed that the plane in which the structure aligns is inclined at approximately 45° to the direction of ring propagation, which is consistent with the experimental and numerical findings for a free vortex ring (Shariff *et al.* 1994). Then, as the vortex ring evolves to the wall, the plane gradually rotates with an inclined angle from 55° at $t = 20$ to 68° at $t = 25$ in Fig. 4(b,c)

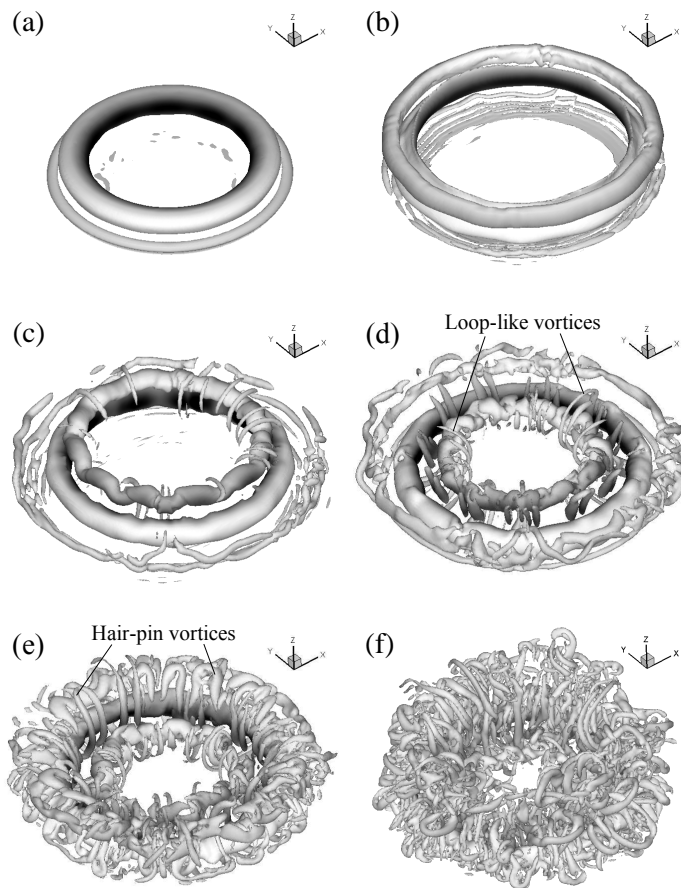


Fig. 2. Evolution of vortical structures visualized by an isosurface of the Q criterion with $Q = 1$ for thin vortex ring: (a) $t = 22.5$, (b) 25.0 , (c) 27.5 , (d) 30.0 , (e) 32.5 , (f) 37.5 .

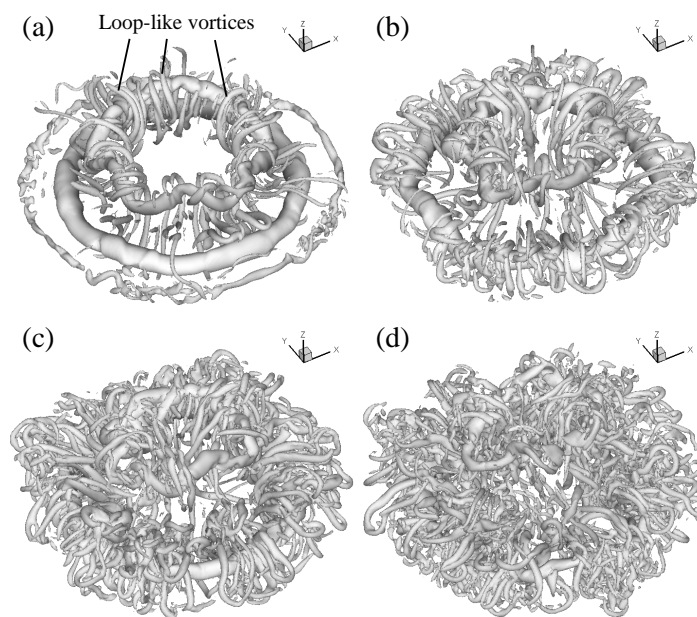


Fig. 3. Evolution of vortical structures visualized by an isosurface of the Q criterion with $Q = 1$ for the thick vortex ring: (a) $t = 35$, (b) 40 , (c) 45 , (d) 50 .

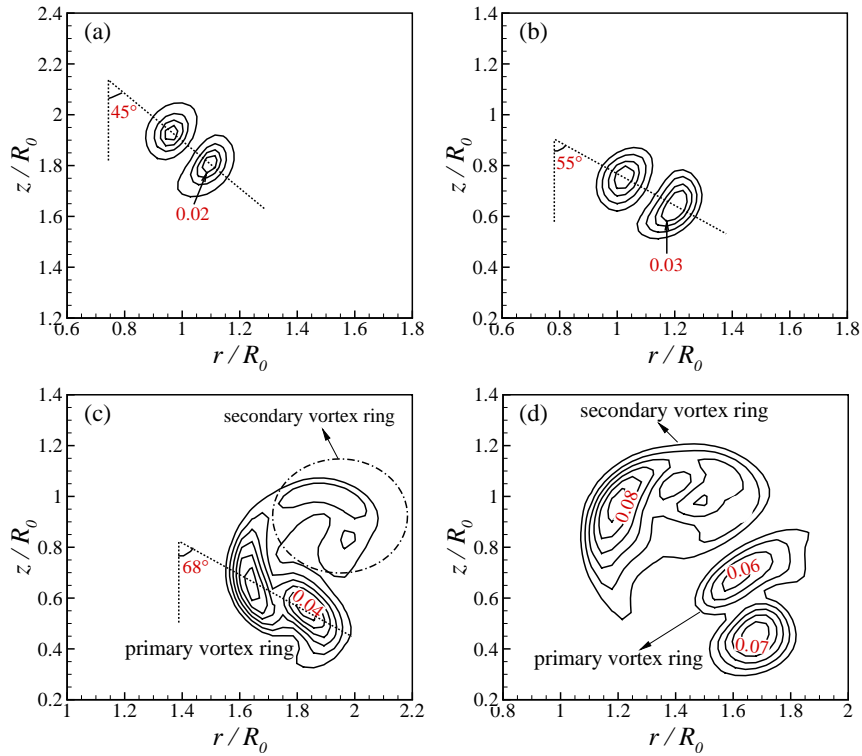


Fig. 4. Evolution of $u_{\theta rms}$ for the thin vortex ring: (a) $t = 15$, (b) 20, (c) 25, (d) 27.5.

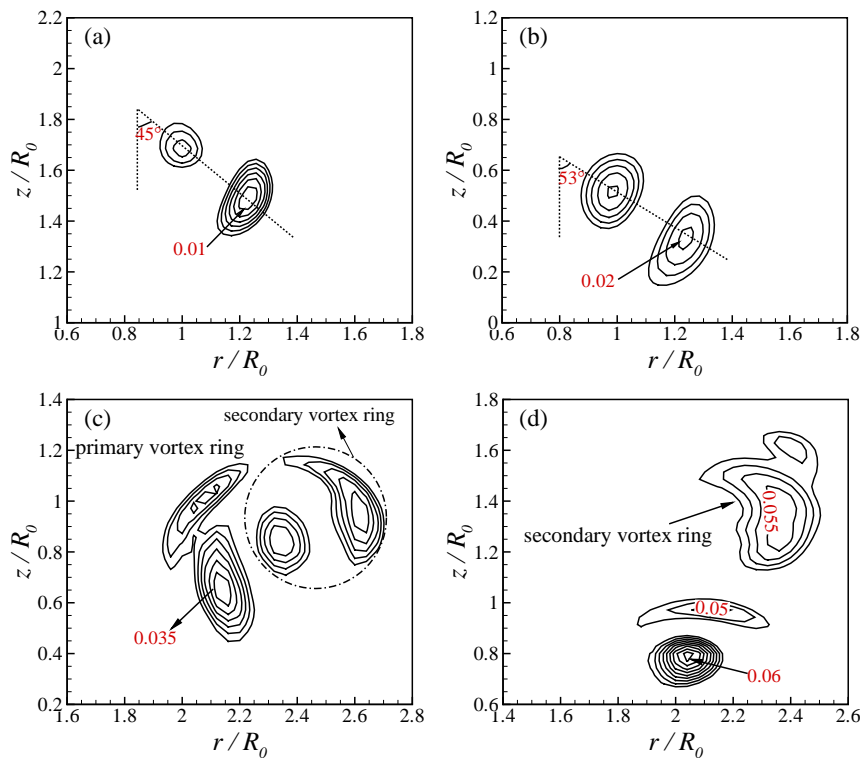


Fig. 5. Evolution of $u_{\theta rms}$ for the thick vortex ring: (a) $t = 15$, (b) 20, (c) 25, (d) 27.5.

due to the wall effect. From the contour values, the magnitude of $u_{\theta rms}$ increases, indicating the

perturbation growth during the ring evolution. Furthermore, the perturbation of $u_{\theta rms}$ for the

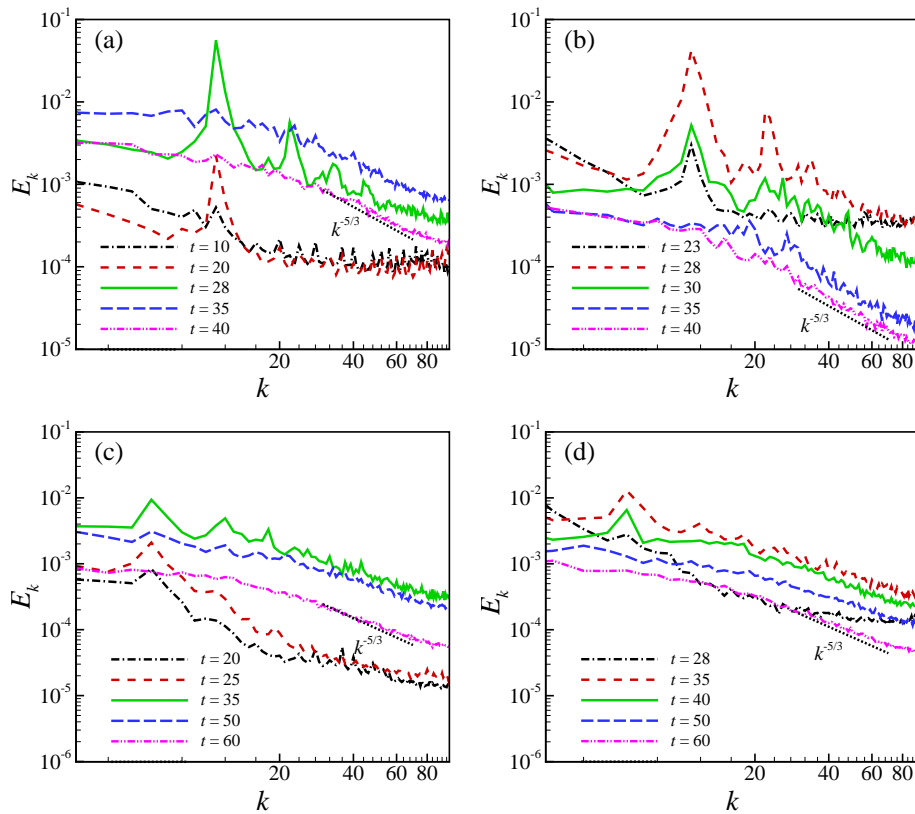


Fig. 6. Modal energies over all the simulated modes at several typical times: (a,c) primary vortex ring, (b,d) secondary vortex ring; (a,b) thin vortex ring case, (c,d) thick vortex ring case.

secondary vortex ring is obviously apparent in Fig. 4(c,d) at $t = 25$ and 27.5 , corresponding to the vortical structures in Fig. 2(b,c). The amplitude of $u_{\theta rms}$ for the secondary ring is larger than one for the primary ring in Fig. 4(d), indicating that the perturbation growth is faster for the secondary ring. In order to compare the perturbation growth for the thin and thick vortex ring cases, Fig. 5. shows the contours of $u_{\theta rms}$ for the thick vortex ring. It can be seen that the increase of inclined angle and rotation of the plane are similar to the thin ring case. While the amplitude of $u_{\theta rms}$ for both the primary and secondary rings is smaller than that for the thin ring case at the same time, indicating the perturbation of the thick vortex rings grow more slowly.

To quantitatively study the instability of vortex rings, Fig. 6. shows the perturbation energy E_k (Shariff *et al.* 1994, Archer *et al.* 2008) in different azimuthal modes, where k represents the wavenumber of the instability modes for the vortical structures. The perturbation corresponding to $k = 0$ is a simple displacement of the entire core and can be associated with

Crow's long-wavelength instability. The higher order bending modes with $k \geq 1$ have a more complicated radial structure leading to internal deformations of the vortical core. For the thin primary vortex ring in Fig. 6(a), the modal energies are relatively weak at $t = 10$ and a peak occurs for $k = 11$ at $t = 20$. This indicates that the dominant mode is $k = 11$, consistent with the theoretical estimate of the dominant mode approximately $k = 2.26/\sigma_0$ (Shariff *et al.* 1994). Then, the E_k is amplified considerably for all the modes and the peaks of subharmonics $k = 22, 33,$ and 44 are apparent at $t = 28$. With the evolution of the vortex ring, the energies at the dominant mode and its subharmonics are transferred to other modes. The modal energies are amplified with temporal evolution and decay smoothly with k at $t = 35$. Furthermore, with the vortices breaking into small-scale ones, the modal energies are gradually reduced at $t = 40$. It is reasonably identified that the law of energy decay follows a characteristic $k^{-5/3}$ law, indicating that the vortical flow has become turbulent state (Laporte and Corjon 2000; Rees *et al.* 2012). Further, Fig. 6(b) shows the modal energies of secondary vortex ring. Similar to the

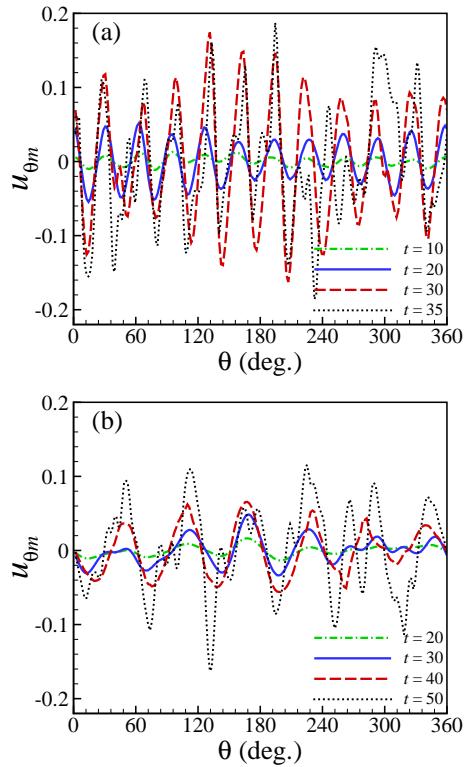


Fig. 7. Axial flow of primary vortex rings: (a) thin vortex ring, (b) thick vortex ring.

development of modal energies for the primary ring, the dominant mode $k = 11$ exhibits a peak at $t = 23$ and its subharmonics are apparent at $t = 28$. Then, the energy transfers among the modes with the evolution of vortical flow and finally exhibits the $-5/3$ decay law at $t = 40$.

The development of modal energies for the primary and secondary rings is shown in Fig. 6(c,d) for the thick ring case. Similar to the thin ring case, the peaks of E_k reasonably correspond to the dominant mode $k = 6$ and its subharmonic modes $k = 12$ and 18 . With the evolution of vortical flow, the energy decay follows the $-5/3$ law, such as the profile at $t = 60$. Moreover, it is also seen that the peak values of dominant mode and its subharmonic modes for the thick ring are smaller than those for the thin ring, which is related to the fact that the instability growth for the thick ring is slower than that for the thin ring.

Further, the axial flow, which represents the circumferential flow along the axis of the vortex core (Maxworthy 1977), is investigated because it is related to the vortex ring evolution to turbulent state (Archer *et al.* 2008). As the axial flow reaches maximum at the center of the vortex core, the axial flow $u_{\theta m}$ and the core center

can be determined by the interpolation from the local azimuthal velocity u_{θ} . Fig. 7 shows the azimuthal distributions of axial flow of the primary ring at several instants. As shown in Fig. 7(a) for the thin ring, the amplitude of $u_{\theta m}$ is relatively small at $t = 10$ and grows quickly with time to generate a pronounced axial flow, such as at $t = 30$ and 35 . It is also seen that the number of wave-like curve is 11, consistent with the dominant azimuthal mode $k = 11$. Similarly, as shown in Fig. 7(b) for the thick ring, the axial flow grows quickly and the number of wave-like curve also corresponds to the dominant azimuthal mode $k = 6$. Compared to the temporal evolution of the axial flow for the thin and thick rings, it is reasonably identified that the growth rate of axial flow for the thin ring is faster than that for the thick ring. Moreover, the axial flow should be due to an azimuthal pressure gradient (Naitoh *et al.* 2002), which is associated with the growth of azimuthal instability and the relevant core stretching of vortex ring.

4.3 Flow behaviours in turbulent state

Based on the preceding discussion, after the vortex rings breaking into small-scale vortices, the transition from laminar to turbulent state occurs. To investigate the flow evolution and the relevant turbulent behaviour, we analyse the total turbulent kinetic energy (TKE), which is defined as

$$TKE = \frac{1}{2} \int (\mathbf{u}' \cdot \mathbf{u}') dV, \quad (14)$$

where \mathbf{u}' represents the velocity fluctuation and is defined as $\mathbf{u}' = \bar{\mathbf{u}} - \langle \bar{\mathbf{u}} \rangle$, and the integral domain is the whole flow field

Figure 8 shows the evolution of total TKE and enstrophy of the wrapping vortices, respectively. Here the behaviour relevant to the TKE is first analysed. For the thin vortex ring, the TKE remains nearly zero, corresponding to the laminar flow state. Then the TKE gradually grows at approximately $t = 24$ and rapidly reaches its maximum at approximately $t = 40$, representing the flow transition to turbulence (Sreedhar and Ragab 1994; Ragab and Sreedhar 1995). Subsequently, in the turbulent state of vortical flow evolution, the TKE continuously decays due to viscous effect. For the thick ring, the TKE evolves slowly with respect to the thin ring case and reaches its maximum at approximately $t = 54$. Moreover, the strength of TKE for the thick ring is smaller than that for the thin ring, consistent with the behaviour relevant to the modal energies in Fig. 6.

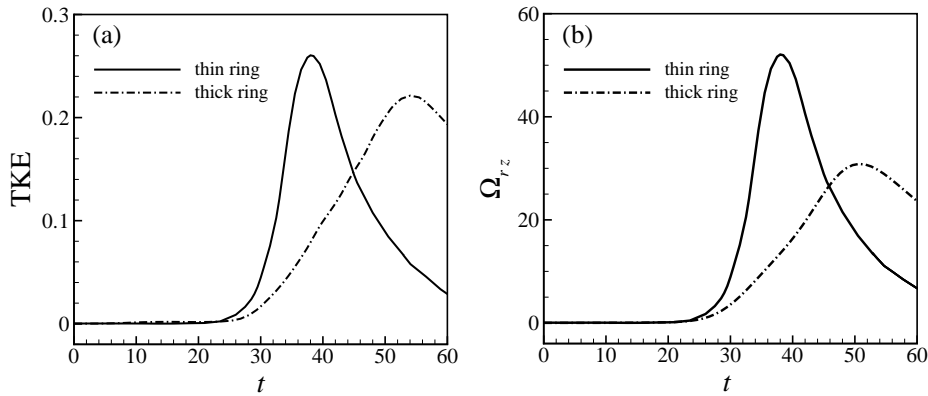


Fig. 8. Evolution of (a) total turbulent kinetic energy and (b) enstrophy for the vortices wrapping around the vortex rings in the whole domain.

The formation and evolution of the vortices wrapping around the vortex rings, such as the loop-like and hair-pin vortices, play an important role in fl w transition from laminar to turbulent state (Ragab and Sreedhar 1995; Archer *et al.* 2008). Here, we will quantitatively examine the intrinsic connection of the wrapping vortices with the vortical fl w evolution and transition to turbulence. Based on our careful analysis of the vortical structures described in 4.1, the wrapping vortices are mainly contributed by the vorticity components in the radial and vertical directions, i.e. ω_r and ω_z . Consequently, the strength of the wrapping vortices can be measured by the total enstrophy in the whole fl w field which is expressed as

$$\Omega_{rz} = \frac{1}{2} \int (\omega_r^2 + \omega_z^2) dV. \quad (15)$$

Figure 8(b) shows the evolution of Ω_{rz} . It is interesting to notice that the profile of Ω_{rz} and TKE in Fig. 8(a) exhibit the similar manner. The generation of Ω_{rz} due to the loop-like and hair-pin vortices is associated with the evolution of TKE. This behaviour confirm that the intrinsic connection of the wrapping vortices with the vortical fl w transition to turbulence.

5. CONCLUSION

In this study, a vortex ring impinges on a fl a wall at two different core thicknesses is investigated. After the secondary vortex ring is generated on the wall, it is convected inward to the center area of the primary ring for the thin vortex ring case and moves far away from the wall for the thick ring case. Finally, the interactions of the vortical structures in the fl w lead to the breakdown of large vortical structures into small-scale vortices and the fl w transition from

laminar to turbulent regime.

The development of azimuthal instability in the primary and secondary vortex rings is investigated. It is identify that the dominant modes for the thin and thick vortex rings are $k = 11$ and $k = 6$ respectively, consistent with the theoretical estimate $k = 2.26/\sigma_0$ by Shariff *et al.* (1994). Moreover, it is found that the azimuthal instability for the thick ring grows and decays more slowly than that for the thin ring. The fl w transition to turbulence is marked by the $-5/3$ decay law of perturbation kinetic energy spectra.

Finally, we analyse the turbulent fl w after the breakdown of the vortical structures. The turbulent kinetic energy grows rapidly during the transition process, until the vortical structures become fully turbulent. It is identify that the loop-like and hair-pin vortices play an important role in transferring the fl w to turbulence, consistent with the isolated vortex ring evolution by Archer *et al.* (2008).

REFERENCES

- Adrian, R. J. (2007). Hairpin vortex organization in wall turbulence. *Phys. Fluids* 19, 041301.
- Archer, P. J., T. G. Thomas and G. N. Coleman (2008). Direct numerical simulation of vortex ring evolution from the laminar to the early turbulent regime. *J. Fluid Mech.* 598, 201–226.
- Archer, P. J., T. G. Thomas and G. N. Coleman (2010). The instability of a vortex ring impinging on a free surface. *J. Fluid Mech.* 642, 79–94.
- Bergdorf, M., P. Koumoutsakos and A. Leonard (2007). Direct numerical simu-

- lation of vortex rings at $Re_{\square} = 7500$. *J. Fluid Mech.* 581, 495–505.
- Boldes, U. and J. C. Ferreri (1973). Behavior of vortex rings in the vicinity of a wall. *Phys. Fluids* 16, 2005–2006.
- Cheng, M., J. Lou and L. S. Luo (2010). Numerical study of a vortex ring impacting a flat wall. *J. Fluid Mech.* 660, 430–455.
- Chu, C. C., C. T. Wang and C. S. Hsieh (1993). An experimental investigation of vortex motions near surfaces. *Phys. Fluids A* 5, 662–676.
- Couch, L. D. and P. S. Krueger (2011). Experimental investigation of vortex rings impinging on inclined surfaces. *Exp. Fluids* 51, 1123–1138.
- Crow, S. C. (1970). Stability theory for a pair of trailing vortices. *AIAA J.* 8, 2172–2179.
- Dazin, A., P. Dupont and M. Stanislas (2006). Experimental characterization of the instability of the vortex ring. Part I: Linear phase. *Exp. Fluids* 40, 383–399.
- Fabris, D., D. Liepmann and D. Marcus (1996). Quantitative experimental and numerical investigation of a vortex ring impinging on a wall. *Phys. Fluids* 8, 2640–2649.
- Gan, L., T. B. Nickels and J. R. Dawson (2011). An experimental study of a turbulent vortex ring: a three-dimensional representation. *Exp. Fluids* 51, 1493–1507.
- Gossler, A. A. and J. S. Marshall (2001). Simulation of normal vortex-cylinder interaction in a viscous fluid. *J. Fluid Mech.* 431, 371–405.
- Hon, T. L. and J. D. A. Walker (1991). Evolution of hairpin vortices in a shear flow. *Comput. Fluids* 20, 343–358.
- Krishnamoorthy, S., A. A. Gossler and J. S. Marshall (1999). Normal vortex interaction with a circular cylinder. *AIAA J.* 37, 50–57.
- Krishnamoorthy, S. and J. S. Marshall (1998). Three-dimensional blade-vortex interaction in the strong vortex regime. *Phys. Fluids* 10, 2828–2845.
- Laporte, F. and A. Corjon (2000). Direct numerical simulations of the elliptic instability of a vortex pair. *Phys. Fluids* 12, 1016–1031.
- Lim, T. T., T. B. Nickels and M. S. Chong (1991). A note on the cause of rebound in the head-on collision of a vortex ring with a wall. *Exp. Fluids* 12, 41–48.
- Liu, C., L. Chen (2011). Parallel DNS for vortex structure of late stages of flow transition. *Comput. Fluids* 45, 129–137.
- Masuda, N., J. Yoshida, B. Ito, T. Furuya and O. Sana (2012). Collision of a vortex ring on granular material. Part I. Interaction of the vortex ring with the granular layer. *Fluid Dyn. Res.* 44, 015501.
- Maxworthy, T. (1977). Some experimental studies of vortex rings. *J. Fluid Mech.* 81, 465–495.
- Moin, P., K. Squires and L. S. Cabot (1991). A dynamic subgrid-scale model for compressible turbulence and scalar transport. *Phys. Fluids A* 3, 2746–2757.
- Naitoh, T., N. Fukuda, T. Gotoh, H. Yamada and K. Nakajima (2002). Experimental study of axial flow in a vortex ring. *Phys. Fluids* 14, 143–149.
- Orland, P. (1990). Vortex dipole rebound from a wall. *Phys. Fluids A* 2, 1429–1436.
- Orlandi, P. and R. Verzicco (1993). Vortex rings impinging on walls: axisymmetric and three-dimensional simulations. *J. Fluid Mech.* 256, 615–646.
- Ragab, S. and M. Sreedhar (1995). Numerical simulation of vortices with axial velocity deficits. *Phys. Fluids* 7, 549–558.
- Rees, W. M., F. Hussain and P. Koumoutsakos (2012). Vortex tube reconnection at $Re = 104$. *Phys. Fluids* 24, 075105.
- Ren, H., G. X. Zhang and H. S. Guan (2015). Three-dimensional numerical simulation of a vortex ring impinging on a circular cylinder. *Fluid Dyn. Res.* 47, 025507.
- Saffman, P. (1978). The number of waves on unstable vortex rings. *J. Fluid Mech.* 84, 625–639.
- Shariff, K. and A. Leonard (1992). Vortex rings. *Annu. Rev. Fluid Mech.* 24, 235–279.
- Shariff, K., R. Verzicco and P. Orlandi (1994). A numerical study of three-dimensional vortex ring instabilities: viscous corrections and early nonlinear stage. *J. Fluid Mech.* 279, 351–375.
- Sreedhar, M. and S. Ragab (1994). Large eddy simulation of longitudinal stationary vortices. *Phys. Fluids* 6, 2501–2514.

- Swearingen, J. D., J. D. Crouch and R. A. Handler (1995). Dynamics and stability of a vortex ring impacting a solid boundary. *J. Fluid Mech.* 297, 1–28.
- Walker, J. D. A., C. R. Smith, A. W. Cerra and T. L. Doligalski (1987). The impact of a vortex ring on a wall. *J. Fluid Mech.* 181, 99–140.
- Widnall, S. E., D. B. Bliss and C. Y. Tsai (1974). The instability of short waves on a vortex ring. *J. Fluid Mech.* 66, 35–47.
- Widnall, S. E. and J. P. Sullivan (1973). On the stability of vortex rings. *Proc. R. Soc. Lond. A* 332, 335–353.
- Widnall, S. E. and C. Y. Tsai (1977). The instability of the thin vortex ring of constant vorticity. *Phil. Trans. R. Soc. Lond. A* 287, 273–305.
- Yoshida, J., N. Masuda, B. Ito, T. Furuya O. Sana (2012). Collision of a vortex ring on granular material. Part II. Erosion of the granular layer. *Fluid Dyn. Res.* 44, 015502.